Paleoceanography and Paleoclimatology

RESEARCH ARTICLE
10.1029/2024PA004939

Special Collection:
Illuminating a Warmer World: Insights from the Paleogene

Tropical Atlantic Temperature and Hydrologic Change During the Paleocene-Eocene Thermal Maximum

Chels Howard[1,2], Donald E. Penman[1], Jiang Zhu[3], Dustin T. Harper[4], Dennis L. Newell[1], and Richard D. Norris[5]

[1]Department of Geosciences, Utah State University, Logan, UT, USA, [2]Now at New Mexico Environment Department, Santa Fe, NM, USA, [3]NSF National Center for Atmospheric Research, Boulder, CO, USA, [4]Geology & Geophysics, University of Utah, Logan, UT, USA, [5]Scripps Institute of Oceanography, UC San Diego, San Diego, CA, USA

Abstract The Paleocene-Eocene Thermal Maximum (PETM, ~56 million years ago) is among the best-studied climatic warming events in Earth history and is often compared to projected anthropogenic climate change. The PETM is characterized by a rapid negative carbon isotope excursion and global temperature increase of 4–5°C, accompanied by changes in spatial patterns of evaporation and precipitation in the global hydrologic cycle. Recent climate model reconstructions suggest a regionally complex and non-linear response of one important aspect of global hydrology: enhanced moisture flux from the low-latitude ocean. In this study, we use the elemental and stable isotope geochemistry of surface-dwelling planktic foraminifera from a low-latitude Atlantic deep-sea sedimentary record (IODP Site 1258) to quantify changes in sea-surface temperature (SST) and salinity. Foraminiferal Mg/Ca and $\delta^{18}O$ values are interpreted with a Bayesian forward proxy system model to reconstruct how SST and salinity changed over the PETM at this site. These temperature and salinity reconstructions are then compared to recent climate model simulations of Eocene warming. Our reconstructions indicate 4.9 $\pm \frac{0.4}{0.5}$ °C of warming, in excellent agreement with estimates from other tropical locations and modeled PETM warmth. The regional change in salinity is not as straightforward, demonstrating a slight decrease at extreme pCO_2 forcing (a reversal of the modeled sense of change under moderate pCO_2 forcing) in both model and proxy reconstructions. The cause of this non-linear response is unclear but may relate to increased South American continental runoff or shifts in the Inter-Tropical Convergence Zone.

Key Points:

- Planktonic foraminiferal Mg/Ca and $\delta^{18}O$ are used to reconstruct warming and salinity change over the Paleocene-Eocene Thermal Maximum (PETM) in the tropical Atlantic
- Reconstructed warming of 4.9°C is similar to other low-latitude sites, and consistent with modeled PETM warmth
- Both proxy reconstructions and climate modeling suggest complex, non-linear hydrologic response to PETM warming

Supporting Information:

Supporting Information may be found in the online version of this article.

Correspondence to:

D. E. Penman,
donald.penman@usu.edu

Citation:

Howard, C., Penman, D. E., Zhu, J., Harper, D. T., Newell, D. L., & Norris, R. D. (2025). Tropical Atlantic temperature and hydrologic change during the Paleocene-Eocene Thermal Maximum. *Paleoceanography and Paleoclimatology*, *40*, e2024PA004939. https://doi.org/10.1029/2024PA004939

Received 31 MAY 2024
Accepted 16 FEB 2025

Author Contributions:

Conceptualization: Donald E. Penman
Data curation: Chels Howard, Donald E. Penman
Formal analysis: Donald E. Penman, Dustin T. Harper, Dennis L. Newell
Funding acquisition: Donald E. Penman
Investigation: Chels Howard, Donald E. Penman, Dustin T. Harper, Dennis L. Newell
Methodology: Donald E. Penman, Jiang Zhu, Dustin T. Harper, Dennis L. Newell
Project administration: Donald E. Penman

1. Introduction

1.1. The PETM

The Paleocene-Eocene Thermal Maximum (PETM, ~56 million years ago) is one of the most prominent global warming events in geologic history. Due to its rapidity, magnitude of carbon emissions, and global extent, the PETM has been intensely studied as a potential analog to modern, anthropogenic climate change (Kennett & Stott, 1991; Koch et al., 1992; Kozdon et al., 2013; McInerney & Wing, 2011; Nunes & Norris, 2006; Zachos et al., 2003, 2005). During the PETM's geologically rapid onset of less than 10,000 years (Kirtland Turner & Ridgwell, 2016; Zeebe et al., 2016), increasing atmospheric pCO_2 caused rapid changes in global climate (Tierney et al., 2022; Zachos et al., 2003), seawater chemistry (Gutjahr et al., 2017; Penman et al., 2014; Zachos et al., 2005), ocean circulation (Nunes & Norris, 2006; Zeebe & Zachos, 2007), and biota (McInerney & Wing, 2011). Global mean surface temperatures rose by 5.6 $\pm \frac{0.3}{0.2}$ °C (Tierney et al., 2022) and up to 5–8°C in the Arctic (McInerney & Wing, 2011; Sluijs et al., 2006, 2008). PETM warmth was sustained for over 100,000 years before climate returned to pre-event levels (Farley & Eltgroth, 2003; Röhl et al., 2007; Zachos et al., 2003). This event is widely attributed to the rapid release of carbon into the atmosphere and oceans, although the cause of the release in CO_2 and its source are debated, ranging from wildfires (Kurtz et al., 2003) to melting of methane hydrates (Dickens et al., 1995, 1997; Katz et al., 1999; Kvenvolden, 1993; Zeebe et al., 2009) to volcanic activity (Svensen et al., 2004, 2010; Westerhold et al., 2009). The PETM can be compared to current climate change as both involve CO_2 released rapidly into the atmosphere (Gutjahr et al., 2017; Hönisch et al., 2012), although anthropogenic activities have released carbon significantly faster than during the PETM (Kirtland Turner, 2018; Zeebe et al., 2016).

Two important impacts of greenhouse-driven warming are increasing temperatures and a resulting intensification and modification of the global hydrologic cycle. Warming is thought to drive an acceleration of global hydrologic flux as well as an increase in extreme weather events (Myhre et al., 2019). Changes in precipitation and

Resources: Donald E. Penman, Dustin T. Harper, Dennis L. Newell, Richard D. Norris
Software: Jiang Zhu, Dustin T. Harper
Supervision: Donald E. Penman
Validation: Donald E. Penman, Dustin T. Harper, Dennis L. Newell
Visualization: Chels Howard, Dustin T. Harper
Writing – original draft: Chels Howard
Writing – review & editing: Donald E. Penman, Jiang Zhu, Dustin T. Harper, Dennis L. Newell, Richard D. Norris

evaporation have often been framed as a wet-get-wetter, dry-get-drier response (Burke et al., 2006; Carmichael et al., 2017; Held & Soden, 2005; Manabe et al., 2004). Areas where drought is common are expected to experience intensified and longer drought seasons, and areas prone to flood will see an increase in large floods due to a predicted increase in large storms including tropical cyclones (Burke et al., 2006; Gregory et al., 1997; Manabe et al., 2004; Wang, 2005). In the near future, changes to the hydrologic cycle have the potential to affect food resources by altering the distribution of precipitation, fire and flood risk, and other hazards (IPCC, 2023). Studying past instances of global warming, such as the PETM, offer an opportunity to ground-truth predictions of future climate change.

1.2. Geochemistry of Foraminifera

The geochemistry of planktonic foraminifera preserved in deep-sea sediments can be used to reconstruct the ancient environmental properties of the seawater in which they lived. Foraminifera build their $CaCO_3$ shells from dissolved ions in the surrounding seawater and their isotopic and chemical composition are affected by paleo-environmental conditions. The Mg/Ca ratio of planktic foraminiferal shells is an established proxy for reconstructing ancient sea surface temperatures (Delaney et al., 1985; Lear et al., 2000; Mashiotta et al., 1999; Wade et al., 2012) with some significant but well-understood secondary controls like pH and salinity (Evans et al., 2016). The oxygen stable isotope composition ($\delta^{18}O$ value) of foraminiferal $CaCO_3$ is primarily a function of the oxygen isotopic composition and temperature of ancient sewater (e.g., Pearson, 2012). Combining paired measurements of Mg/Ca and $\delta^{18}O$ from foraminiferal calcite can simultaneously constrain ancient sea surface temperatures and the $\delta^{18}O$ of ancient seawater (Zachos et al., 2003).

The $\delta^{18}O$ value of ancient seawater is useful for reconstructions of the ancient hydrologic cycle because fractionation of oxygen isotopes also occurs during evaporation and precipitation. Because evaporation from the sea surface preferentially takes up the lighter isotope (^{16}O), this leaves surface water enriched in the heavier isotope (^{18}O) (e.g., Horita et al., 2008). Increased precipitation therefore lowers surface water $\delta^{18}O$, and increased evaporation leaves surface waters with higher $\delta^{18}O$. At a global scale, as water is evaporated at low latitudes and transported polewards, it becomes increasingly lower in $\delta^{18}O$ (Dee et al., 2023). However, much of the water evaporated near the equator falls back on the intertropical convergence zone (ITCZ) and is thus recycled at low-latitudes. This internal low latitude evaporation-precipitation cycle accounts for more than 30% of global precipitation (Liu et al., 2020).

The global gradient in the $\delta^{18}O$ of surface seawater is a reflection of the global flux of water vapor from regions of net evaporation (such as the subtropics) and net precipitation (the high latitudes and the ITCZ). An intensification of the hydrologic cycle (as is expected under a warming climate; Carmichael et al., 2017; Evans et al., 2016; Held & Soden, 2000, 2005) would be expected to amplify spatial differences of seawater $\delta^{18}O$, following a wet-get-wetter, dry-get-drier response. Since the balance of evaporation and precipitation also largely controls the sea-surface salinity (SSS) gradients in the ocean, $\delta^{18}O$ and salinity are highly correlated in the modern ocean and past changes in seawater $\delta^{18}O$ can be used to estimate changes in SSS.

Temperature and salinity over the PETM have been previously estimated at other sites by geochemically analyzing the Mg/Ca and $\delta^{18}O$ values in foraminiferal shells (e.g., Evans et al., 2013; Zachos et al., 2003). In this contribution, we extend these techniques to the tropical Atlantic ocean (Site 1258), a region that recent climate modeling (e.g., Zhu et al., 2020) suggests was particularly susceptible to hydrologic change during PETM warming (Figure 1). Site 1258 is located (present and reconstructed latitude 9.5° N) at the northern seasonal extent of the ITCZ in a region of negative annual net precipitation minus evaporation (P-E). A simple conceptual model would predict a further decrease in P-E with warming (the "dry-get-drier" response) which would manifest as a decrease in seawater $\delta^{18}O$. We aim to test this hypothesis using foraminiferal Mg/Ca and $\delta^{18}O$ in comparison to recent isotope-enabled climate modeling (Zhu et al., 2020).

2. Materials and Methods

2.1. Samples

The samples used in this study are from Ocean Drilling Program (ODP) Site 1258 (Hole C), on Demerara Rise in the Atlantic Ocean off the northeastern coast of South America (Erbacher et al., 2004). The Paleocene-Eocene boundary occurs within Lithostratigraphic Unit II (Erbacher et al., 2004), a nannofossil chalk with

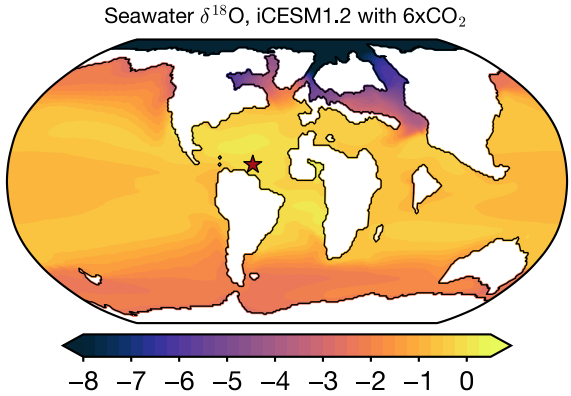

Figure 1. Site 1258 (red star) location on Eocene paleogeography, with surface water δ^{18}O from iCESM 1.2 modeling (Zhu et al., 2020). Units: ‰, VSMOW.

foraminifera. The PETM-aged samples used in this study were previously collected and analyzed for benthic foraminiferal carbon and oxygen stable isotopes, as reported in Nunes and Norris (2006). The Paleocene-Eocene boundary was clearly identified by a decrease of δ^{13}C values in benthic foraminifera (Nunes & Norris, 2006) and a prominent layer of $CaCO_3$-poor nannofossil chalk (Erbacher et al., 2004) at ∼195.7 meters below seafloor (mbsf). To relate the sample core depths to time, an age model was created by tying variations of δ^{13}C values in bulk carbonate (e.g., carbon isotope excursion (CIE) onset during the PETM) from ODP Site 1262 (Zachos et al., 2005) to that of Site 1258 (Pälike et al., 2014) (Table S1 in Supporting Information S1).

Each sample was sieved to 250–300 μm and specimens of the surface-dwelling planktic foraminifer *Morozovella velascoensis* were handpicked under a binocular microscope. *M. velascoensis* are often used for Paleogene paleoclimatological reconstructions because of their abundance in tropical deep-sea sediments, mixed-layer depth habitat required by their algal photosymbionts, and limited stable isotope vital effects (Birch et al., 2012; Cramer et al., 2011; Kelly et al., 2001; Kennett & Stott, 1991; Kozdon et al., 2013). Foraminiferal preservation is variable at Site 1258, so a rigorous screening protocol was developed and employed to ensure that only the best-preserved individuals were used for reconstructions. The preservation screening system is described in full in the supplemental materials, but briefly: shells were first visually screened under a picking microscope for degree of preservation, and then each sample was imaged using a FEI Quanta 650 FEG scanning electron microscope (SEM) at the Microscope Core Facility at Utah State University (USU). 20 to 24 of the most pristine *M. velascoensis* individuals (Figure 2 and SI) were selected for replicate measurements of both Mg/Ca ratio and stable oxygen isotopes (δ^{18}O) using mass spectrometry. These best-preserved individuals exhibit the "frosty" micro-recrystalized preservation typical of Early Cenozoic pelagic chalks (Sexton et al., 2006).

2.2. Geochemical Analyses

Following SEM imaging and screening, samples for Mg/Ca analyses were crushed between two glass slides under the microscope, and shell fragments were cleaned following established chemical cleaning procedures developed for foraminiferal trace metal analyses (Barker et al., 2003). Shell fragments were transferred to clean vials then rinsed and ultrasonicated with alternating MilliQ (MQ) water and methanol to remove any particulate matter and loose clays. After rinsing and sonicating the shells, a reductive step (solution of citric acid and hydrazine in a hot-water bath with repeated sonications) was implemented to remove any metal-oxide coatings on the shells. After rinsing away the reductive solution, an oxidative solution (1% hydrogen peroxide in 0.1 M NaOH in a hot-water bath with repeated sonications) was used to remove any organic material. Cleaned shells were then dissolved in 0.5 M nitric acid prepared with concentrated Optima-grade HNO_3 and MQ ultrapure water. Samples were analyzed for Mg/Ca using an Agilent 8900 triple-quadrupole inductively coupled plasma mass spectrometer (QQQ-ICP-MS) in the USU Department of Geosciences ICP-MS Lab. Samples were calibrated against a series of in-house calibration standards with varying Mg/Ca ratios (analyzed at the beginning and end of runs). All samples were measured in duplicate. In-run and long term external precision was monitored by repeat analysis of NIST 8301f reference standard (Mg/Ca = 2.67 mmol/mol, long-term external precision = ±0.07 mmol/mol or 2.8%, 1 standard deviation).

For δ^{18}O and δ^{13}C analyses, samples consisting of 8–12 individual shells were weighed to ensure they have a mass of between 50 and 100 μg. Oxygen and carbon stable isotope analyses were performed on a Thermo Scientific Delta V Advantage Isotope Ratio Mass Spectrometer coupled to a GasBench II device using continuous-flow techniques in the USU Department of Geosciences Stable Isotope Lab. δ^{18}O and δ^{13}C values were scale normalized relative to Vienna—Pee Dee Belemnite using the international standards NBS-18, NBS-19, and USGS-44. Results for each run were corrected for drift and mass effects using in-house calcite standards (Kim et al., 2015; Paul & Skrzyoek, 2007). δ^{18}O and δ^{13}C values are reported in standard delta notation with errors <0.1‰, 1 standard deviation, determined by repeat analysis of in-house standards.

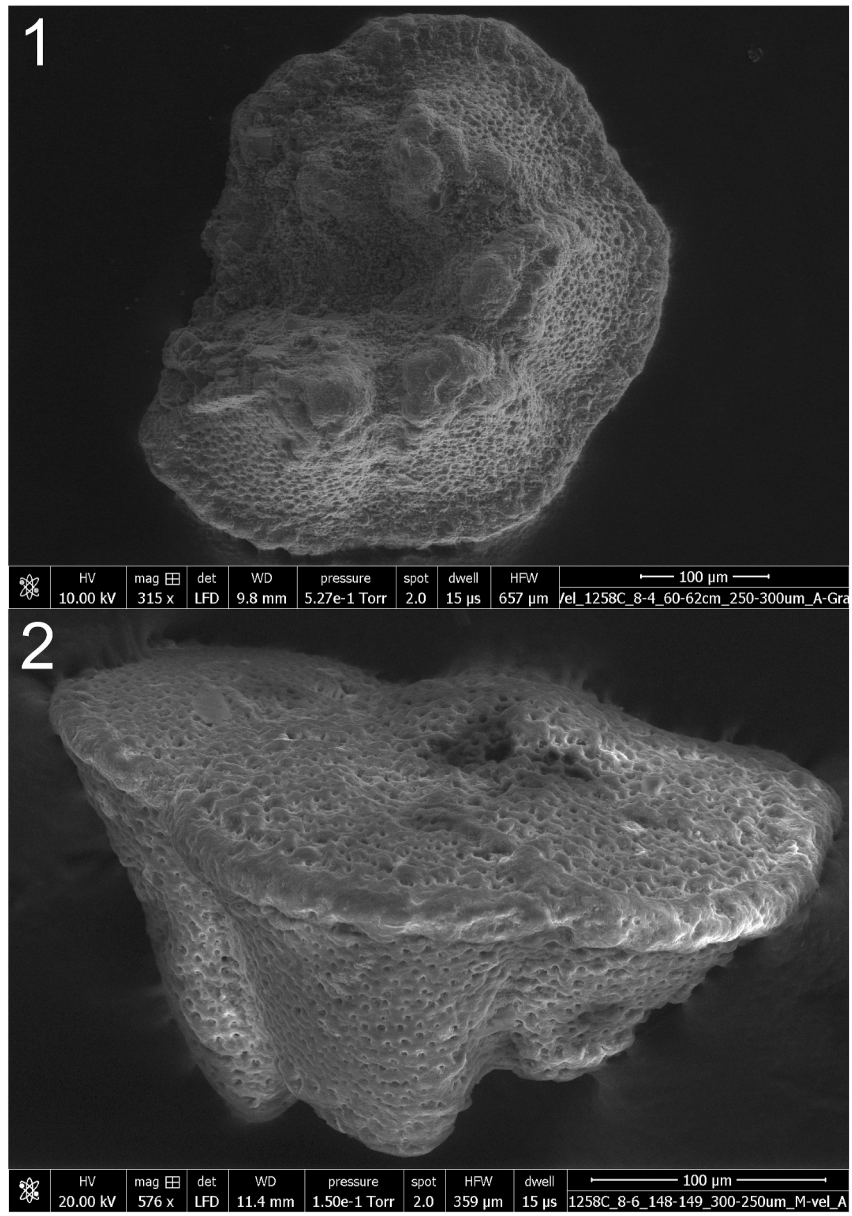

Figure 2. Examples of well-preserved M. velascoensis from Site 1258. 1 is an umbilical view and 2 an edge view of the shell.

2.3. Paleoceanographic Reconstruction

We produce paleoceanographic reconstructions from foraminiferal geochemical data using a new implementation of Bayesian forward Proxy System Modeling (PSM), which is an emerging numerical technique for reconstructing ancient environmental properties from proxy data (Dee et al., 2015; Evans et al., 2013; Tingley et al., 2012). In this approach, environmental and proxy system parameters of influence are represented by probability distributions. These parameter distributions are repeatedly sampled by the model and translated into predicted geochemical proxy values. The model state (i.e., the selected parameter values) is compared to measured data to determine likelihood of the model state. Forward modeling allows for consideration of a full range of possible environmental controls, while accounting for the potential impacts of secondary controls such as diagenesis, which is of particular concern at Site 1258.

Here we use Markov Chain Monte-Carlo (MCMC) methods in a Bayesian hierarchical forward PSM to evaluate the likelihood of proposed environmental model states against foraminifera Mg/Ca and $\delta^{18}O$. Bayes' Theorem states:

$$P(A \mid B) = \frac{P(B \mid A) \times P(A)}{P(B)} \quad (1)$$

where P(A | B) is the probability of A given B (i.e., the posterior probability distributions from the model given the prior distributions and the observed data), P(B | A) is the probability of B given A, or the likelihood of the predicted model given the data, and P(A) and P(B) are the probabilities of A and B, respectively. For our application, P(A) represents the prior probability distributions from which the proposed environmental models are derived, and P(B) represents the probability of the observed data. Bayesian hierarchical modeling generates posterior distributions of parameters proportional to the probability of the environmental models (e.g., Mg/Ca_{sw}, $\delta^{18}O_{sw}$, temperature, salinity) selected from prior distributions, given observations. This allows for integration of observations with differing sampling resolutions and accounts for uncertainties in analytical data, environmental parameters, and sensitivity/calibration parameters (e.g., secular changes in Mg/Ca, diagenesis, and species-specific Mg/Ca-temperature calibration parameters applied to *M. velascoensis*).

The structure used here incorporates a time series environmental model which allows distributions of environmental parameters to change from the initial (prior) parameter values over time. Environmental parameter distributions are allowed to shift with each subsequent time step in the model based on a set of change parameters (cf. Bowen et al., 2020):

$$Y(t) = Y(1) + \varepsilon_Y(t) \quad (2)$$

where Y is the variable, t is the timestep, and ε_Y is an error term, represented in terms of autocorrelation Φ_Y, with τ_Y representing the error precision for a time step size (Δt) of 1:

$$\varepsilon_Y = N\left[\varepsilon_Y(t-1) \times \Phi_Y^{\Delta t},\ \tau_Y \times \frac{(1-\Phi_Y^2)}{(1-\Phi_Y^{2\Delta t})}\right] \quad (3)$$

For concentration parameters we used a more realistic (non-negative) relativistic implementation of ε_Y:

$$Y(t) = Y(1) \times (1 + \varepsilon_Y(t)) \quad (4)$$

In the PSM, foraminiferal Mg/Ca is influenced by temperature, salinity, paleo-seawater Mg/Ca (here, the prior mean is set to 2.5 following Evans et al., 2016; see Table S2 in Supporting Information S1 for all prior distributions used here), and species-specific constants:

$$Mg/Ca_{pf}(t) = \left[\left(\frac{Mg/Ca_{sw}(t)^{H_p}}{Mg/Ca_{sw\ mod}(t)^{H_p}} \times B\right) e^{AT(t)}\right] / (1 - (S(t) - 35) \times C_{sal}) \quad (5)$$

where Mg/Ca_{sw} and $Mg/Ca_{sw\ mod}$ are seawater Mg/Ca (for past and modern, respectively). Species-specific vital effects between foraminiferal shells and the Mg/Ca_{sw} are accounted for with "Hp" of modern foraminiferal analog, *T. sacculifer*, from Haynes et al. (2023). B and A are species-specific Mg/Ca-temperature calibration parameters applied to *M. velascoensis* (B value: Gray & Evans, 2019; A value: Evans et al., 2016; Table S2 in Supporting Information S1). The prior mean for the A-value distribution used here is the all-species regression of Gray and Evans (2019), or 0.061. S is salinity, here with a prior mean of 35 ppt (Table S2 in Supporting Information S1). C_{sal} is the Mg/Ca sensitivity to salinity, with prior mean of 0.042 (Table S2 in Supporting Information S1).

Foraminiferal $\delta^{18}O$ ($\delta^{18}O_{pf}$) is calculated as follows:

$$\delta^{18}O_{pf}(t) = \left[\left(\exp\left(A_{cw} \times 10^3\left(\frac{1}{T(t)} - \frac{1}{297.7}\right) + B_{cw}\right) - 1\right) \times 10^3 + \delta^{18}O_{sw}(t)\right] \times (1 - R_{pc}) + \left(\delta^{18}O_{CPD} \times R_{pc}\right) \quad (6)$$

where $\delta^{18}O_{sw}$ is the local value for $\delta^{18}O$ of seawater (Table S2 in Supporting Information S1; Zhu et al., 2020). R_{pc} is the amount of recrystallization the samples are subjected to, which was visually estimated from foraminifera under the optical microscope and SEM. $\delta^{18}O_{CWE}$ is the assumed secondary calcite endmember $\delta^{18}O$ value. Calcite-water stable isotope fractionation follows the fractionation model of Daëron et al. (2019). The extent of diagenetic alteration of $\delta^{18}O$ values is confirmed by comparing $\delta^{18}O$ and Mg/Ca-based sea-surface temperature (SST) for pre-onset samples. To obtain SST alignment in both proxy systems via traditional inverse calculations, ~20% recrystallization in the measured samples was required (largely consistent with binocular and SEM observations of typical "frosty" sample preservation, Sexton et al., 2006), given an assumed secondary calcite endmember $\delta^{18}O$ value ($\delta^{18}O_{CWE}$ above) of 0.85‰.

Our approach uses Gibbs sampling (Just Another Gibbs Sampler, or JAGS) via rjags (Plummer, 2003) and r2jags (Su & Yajima, 2015) packages in R version 4.2.1 (R Core Team, 2013). The MCMC inversion requires a "burn in" period, which allows the model to converge sufficiently. Convergence during MCMC analysis was monitored using Rubin and Gelman Rhat statistics and traceplots. For the present model inversion, Rhat was <1.02 and effective sampling was >280 for all parameters. The packages used here implement parallel processing for MCMC models using multiple chains (Su & Yajima, 2015). We used nine chains of 150,000 iterations with 50,000 burn-in each to ensure reproducibility and convergence.

The change in SST across the PETM was calculated from averages (means) of pre-PETM baseline posterior distributions (195.83–195.82 mbsf) and peak-PETM warmth posterior distributions (195.01–195.39 mbsf).

For comparison, we also calculated PETM SST and $\Delta\ \delta^{18}O_{sw}$ from foraminifera geochemical data using conventional proxy interpretations (Figure S5 in Supporting Information S1). To calculate SST from Mg/Ca, we followed the recommended corrections and constants of Hollis et al. (2019).

Reconstructed temperature and seawater $\delta^{18}O$ values were compared to climate model results reported by Zhu et al. (2020), who used an isotope-enabled general circulation model (iCESM 1.2) to explore the steady-state climates across a range of atmospheric pCO_2 (1x to 9x preindustrial pCO_2) with Eocene paleogeography. Proxy results from Site 1258 are compared to model output from grid cells within 1 degree of latitude and longitude of the paleolocation of Site 1258 (9.5°N, 42.08°W), based on the same mantle reference frame (Herold et al., 2014) used for the Eocene paleogeography in the iCESM runs.

3. Results

3.1. Geochemical Data

The CIE recorded in planktic foraminifera from Hole 1258C occurs in tandem with that of benthic foraminifera (Nunes & Norris, 2006), at around 195.75 mbsf, with excursion values extending up to 195 mbsf (Figure 3). Across the onset of the PETM (as defined by the CIE), planktic Mg/Ca values increase from a pre-PETM average of 4.6 mmol/mol to 5.9 mmol/mol during the body of the PETM. Planktic $\delta^{18}O$ values ranged from an average of −2.7‰ before the PETM, with a more gradual decrease to a minimum of −3.8‰ during the PETM. Both planktic $\delta^{13}C$ and $\delta^{18}O$ data sets follow the trends of previously published benthic data sets (Nunes & Norris, 2006), with typical planktic-benthic offsets. The planktic-benthic offset in $\delta^{18}O$ value is due to surface-to-deep temperature gradient, while the planktic-benthic $\delta^{13}C$ value offset is caused by the deep water remineralization of surface-seawater-derived low-$\delta^{13}C$ organic matter (the biological carbon pump). Preserved planktic-benthic gradients in both isotopic systems are similar in magnitude to modern gradients, suggesting that primary geochemical signals are preserved in both data sets and minimizing the possible impact of diagenesis on our reconstructions.

The changes in Mg/Ca and $\delta^{18}O$ values over the PETM from Site 1258 are comparable to changes in these parameters documented from other low-latitude pelagic sites such as Site 1209 (Zachos et al., 2003): both sites see a sharp increase in Mg/Ca and a decrease in $\delta^{18}O$, although the $\delta^{18}O$ excursion at Site 1209 is more abrupt, with less fluctuation than observed at Site 1258. The overall similarity of the Mg/Ca and $\delta^{18}O$ records between Sites

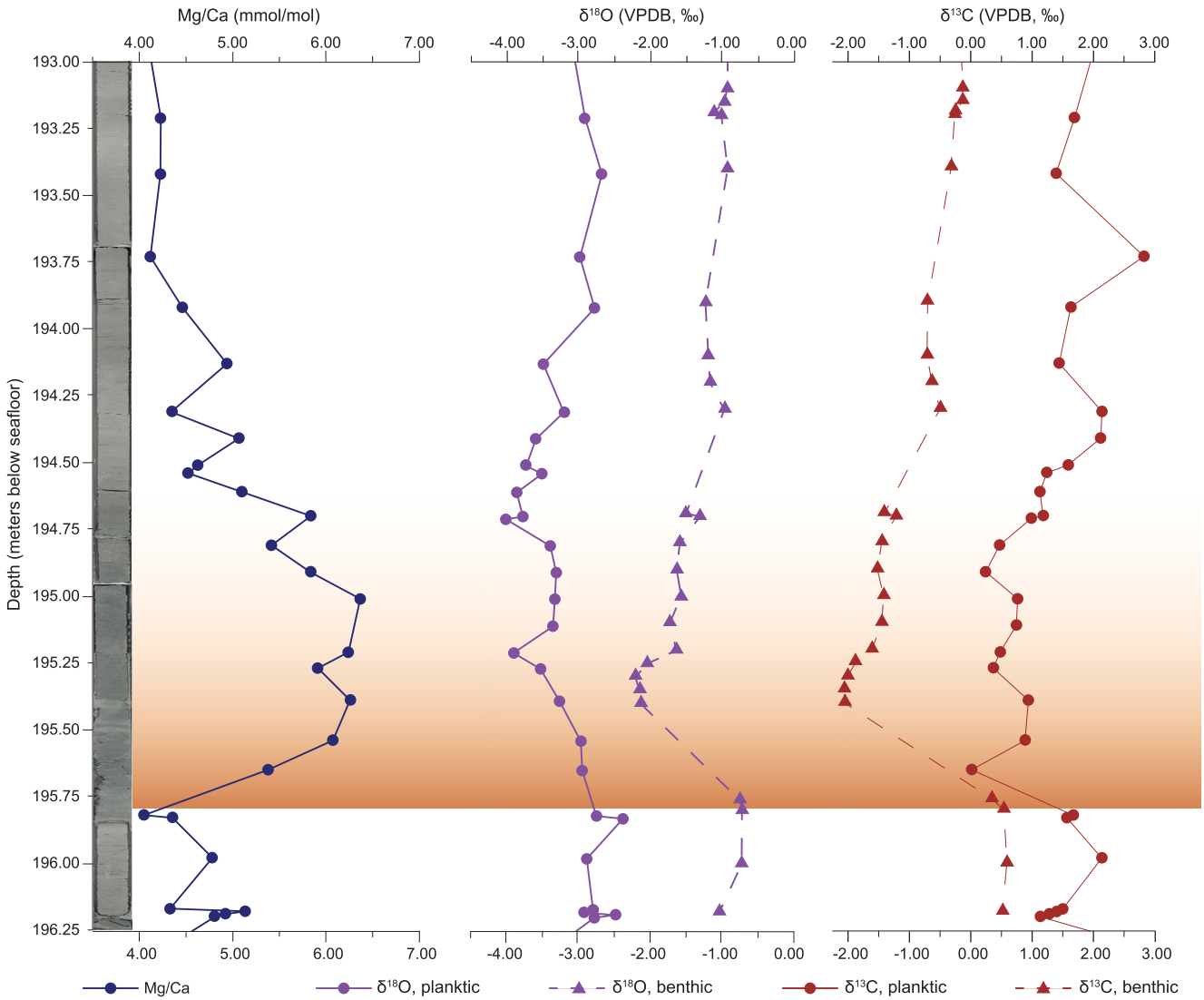

Figure 3. Mg/Ca, $\delta^{18}O$, and $\delta^{13}C$ data measured on well-preserved *Morozovella velascoensis* (labeled "planktic") from Site 1258. The dashed lines represent previously published benthic $\delta^{18}O$ and $\delta^{13}C$ data from Nunes and Norris (2006).

1258 and 1209, both in absolute value and in the sense of change during the PETM, further argues that diagenetic overprinting is minimal.

3.2. Proxy Interpretation

Reconstructions from our MCMC Bayesian PSM indicate pre-PETM absolute baseline SST of 35.7 $\pm \frac{2.1}{1.9}$ °C (95% credible interval, CI), and peak-PETM absolute temperatures of 40.6 $\pm \frac{2.3}{2.2}$ °C (95% CI), followed by a ~50 kyr period of warm temperatures and then a gradual recovery (Figure 4). The amount of relative temperature change (warming) is better constrained than absolute temperatures by our MCMC Bayesian proxy system model, indicating a robust sea surface warming of 4.9 $\pm \frac{0.4}{0.5}$ °C (95% CI). Our calculations of SST using conventional proxy interpretation (Figure S5 in Supporting Information S1) results in SST estimates that are 2–3° cooler before, during, and after the PETM—but suggest a very similar total warming of 4.5°C. Warming observed at Site 1258 is similar in magnitude and timing to SST reconstructions from other low-latitude sites globally (Dunkley-Jones et al., 2013; Frieling et al., 2017; Zachos et al., 2003). PSM Reconstructed seawater $\delta^{18}O$ and salinity values follow a more complex and gradual trajectory, with very little rapid change immediately at the PETM onset, followed by a gradual decrease toward lower seawater $\delta^{18}O$ values (less salinity) during the body of the PETM

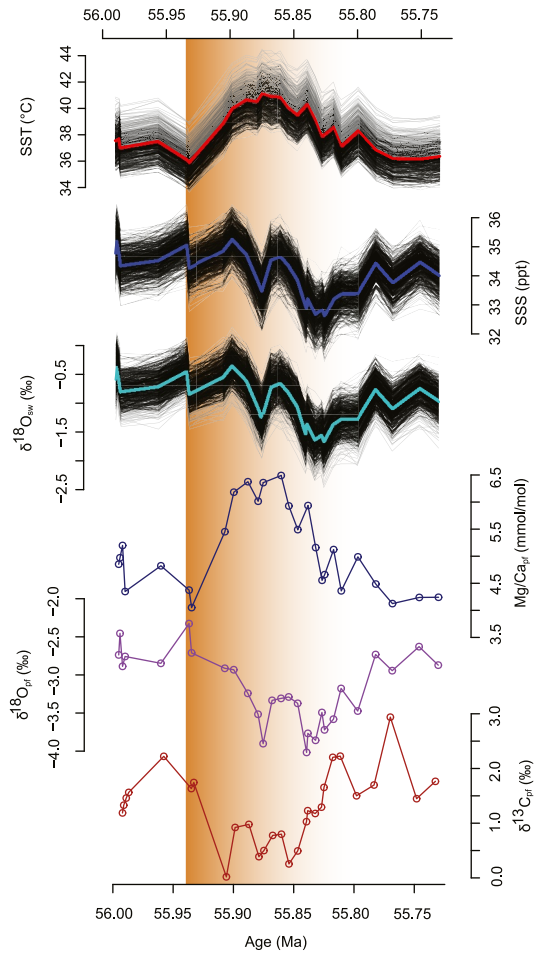

Figure 4. Forward model results. The bottom three panels represent measured data from Site 1258C. The top three panels represent posterior distributions of reconstructed environmental variables, here shown as time series of likely model states from random draws of the many Markov Chain Monte-Carlo iterations, conditioned on measured proxy data. The colored lines represent the median of the time series distributions. The 500 black surrounding lines give an impression of the range of these distributions (i.e., reconstruction uncertainty).

CIE and warm period. After a brief return to saltier conditions, seawater $\delta^{18}O$ and salinity further decrease to their minimum values during the recovery period (as defined by both $\delta^{13}C$ and reconstructed SST), followed by a return to near-pre-event levels. Because the temperature-related component of foraminiferal $\delta^{18}O$ change is almost identical to that considered in the PSM, conventional proxy interpretation reconstructs an almost identical trajectory for seawater $\delta^{18}O$ across the PETM.

4. Discussion

4.1. Tropical Atlantic SST Change During the PETM

Our foraminifera Mg/Ca and $\delta^{18}O$-based reconstructions of Site 1258 sea surface temperatures over the PETM are similar to proxy estimates from other low-latitude sites (e.g., Aze et al., 2014; Dunkley-Jones et al., 2013; Frieling et al., 2017; Hollis et al., 2019; Inglis et al., 2020) and consistent with Eocene climate models predictions (e.g., Tierney et al., 2022; Zhu et al., 2020). We compare our reconstructed temperatures and seawater $\delta^{18}O$ values to climate model simulations from Zhu et al. (2020), using an isotope-enabled general circulation model (iCESM) to explore the steady-state climates across a range of atmospheric pCO_2 and Eocene paleogeography. Our proxy records indicate a pre-PETM SST of ~36°C, which is most consistent with sea-surface temperatures in the region of Site 1258 in iCESM's 6x CO_2 (1680 ppm) scenario of Zhu et al. (2020) (Figure 5a). Our reconstructed pre-PETM baseline SSTs are also similar to global Late Papeocene tropical SST estimates in the compilations of Hollis et al. (2019) Gaskell et al. (2022). Coincident with the CIE, reconstructed SST increases

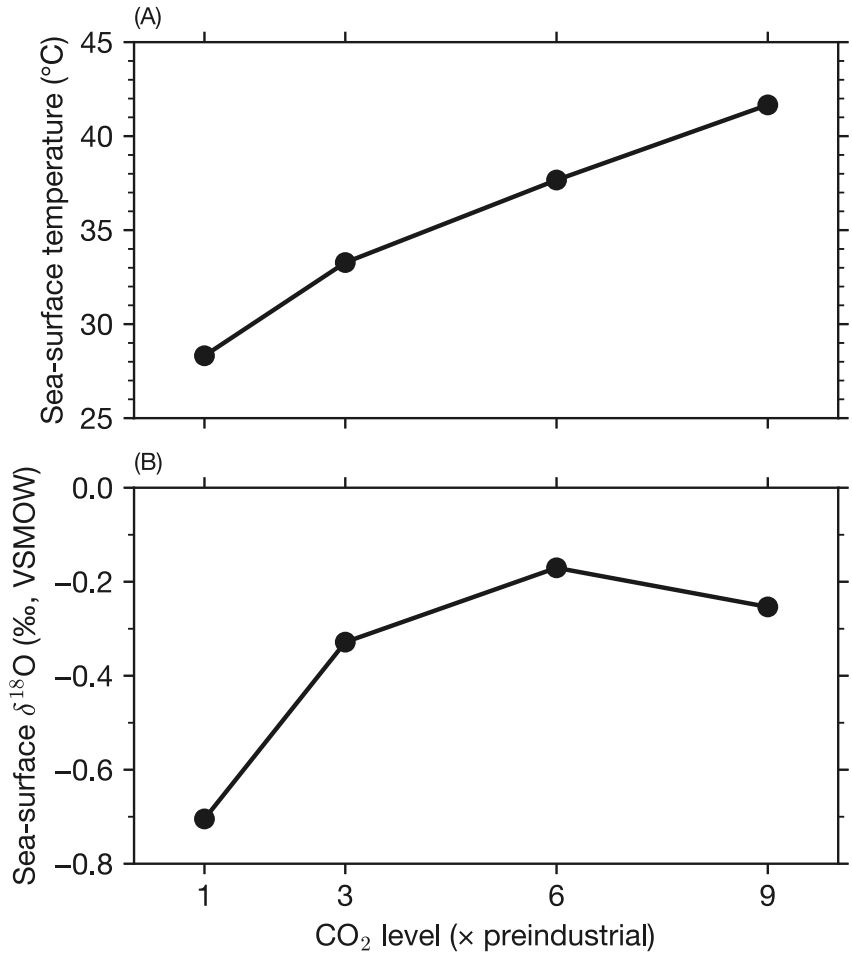

Figure 5. Modeled sea-surface temperature (a) and surface seawater $\delta^{18}O$ (b) for Site 1258 paleolocation from a suite of Eocene simulations across a range of atmospheric pCO_2 (Zhu et al., 2020).

over a few tens of thousands of years, although we caution that this apparently gradual warming (compared to other records) merely reflects the relatively low data resolution (particularly in Mg/Ca) during the very earliest phases of the PETM due to carbonate dissolution. The magnitude of warming across the PETM onset in our reconstruction ($4.9 \pm \frac{0.4}{0.5}$ °C) is in very close agreement with PETM global mean surface temperature change (5.3°C) estimated from a global proxy record compilation by Inglis et al. (2020). Our reconstructed peak PETM temperature around $40.6 \pm \frac{2.3}{2.2}$ °C is even warmer than estimates for the eastern tropical Atlantic (Frieling et al., 2018), but similar to estimates from exceptionally well-preserved PETM foraminifera from Tanzania (Aze et al., 2014), and Mg/Ca-based peak PETM temperatures in the Subtropical Pacific (Harper et al., 2024) These peak temperatures are most consistent with iCESM1.2's regional Site 1258 SSTs in their 9x CO_2 (2,520 ppm) scenario (Figure 5a).

4.2. Tropical Atlantic Hydrologic Change

In both the iCESM1.2 simulations and our proxy reconstructions, the relationship between increasing pCO_2 and changes in Site 1258 surface seawater $\delta^{18}O$/salinity is less straight-forward than the warming response to increasing pCO_2. Previous literature and current CMIP6 models support the hypothesis of wet-gets-wetter and dry-gets-drier in terms of evaporation/precipitation balance (e.g., Carmichael et al., 2017; IPCC, 2023). This means that areas of net evaporation (such as the mid-to low-latitudes and including Site 1258) should experience more intense evaporation with warming, and areas of net precipitation (such as the high-latitudes) will receive more intense precipitation. However, the iCESM1.2 simulations suggest that at very high CO_2 levels, that pattern breaks down in some regions, including the region of Site 1258 (Figure 5b). Comparing conditions at Site 1258

from 1x- to 3x- to 6x- pre-industrial CO_2, seawater $\delta^{18}O$ progressively increases, reflecting increased evaporation (and/or decreased precipitation)—consistent with a dry-get-drier response (Figure 5b). However, in the 9x pre-industrial CO_2 scenario (which features SSTs similar to our PETM reconstructions), the Site 1258 region is predicted to have slightly lower seawater $\delta^{18}O$ than the 6x pre-industrial scenario, reflecting a decrease in evaporation (and/or increase in precipitation)—the opposite of a dry-get-drier response.

At Site 1258, foraminiferal proxy data suggest very little change in seawater $\delta^{18}O$ values at the onset of the PETM, and a decrease in $\delta^{18}O$ during the later stages of the event. Interestingly, there is evidence from higher latitudes for a temporally complex, two-stage global hydrologic response to PETM warming. Pagani et al. (2006) reconstruct lower Arctic Ocean salinity (consistent with enhanced precipitation) in the early stages of the PETM, with a prominent reversal to higher SSS later in the event, indicating a complex evolution of poleward moisture transport over the course of the PETM. Walters et al. (2022) argue for a significant increase in North Sea precipitation at the onset of the PETM but a return to pre-event levels well before the recovery of SST. These records, as well as our new Site 1258 reconstruction, all argue that the response of the hydrologic cycle during the PETM had a more complex evolution than that seen in temperature reconstructions.

The overall $\delta^{18}O_{sw}$ decrease that we see at Site 1258 particularly during the later stages of the PETM is remarkably consistent with the high-CO_2 response modeled between iCESM1.2's 6x and 9x CO_2 comparison: seawater $\delta^{18}O$/salinity exhibits similar behavior to the observed and model data from Site 1258 where the salinity actually decreases at peak pCO_2, in constrast to the expectation from conceptual models that areas of net evaporation see further evaporation (driving higher $\delta^{18}O$/salinity) in warmer climates. Taken together, the model and the data both suggest that a threshold exists at very high pCO_2, when tropical SSTs rise above ~37°C, beyond which the hydrologic response in the Site 1258 region becomes insensitive to further warming, and even reverses.

What could drive a decrease in tropical Atlantic sea-surface $\delta^{18}O$ and salinity values in the extremely warm, high pCO_2 climate of the peak PETM? There is some support from a theoretical perspective for a non-linear hydroclimate response at extreme greenhouse warming, wherein the hydrologic cycle is highly sensitive to changes at modest warming but asymptotically approaches a maximum at extreme surface temperatures (O'Gorman & Schneider, 2008). Other global atmospheric reorganizations have been proposed for super-greenhouse climates that could come play a role during the PETM. Caballero and Huber (2010) propose a global shift to Equatorial atmospheric super-rotation (westerly winds) at near the same equatorial SST threshold that we reconstruct. Abbot et al. (2009) propose that at very high surface temperatures, high-latitude convective clouds amplify polar warming, altering meridional temperature gradients that would certainly effect moisture transport. Either of these global reorganizations could impart a strongly non-linear character to the tropical hydrologic response to warming. However, it is important to note that the decrease in Site 1258 seawater $\delta^{18}O$/salinity (indicating wetter conditions) in the iCESM 1.2 6x–9x comparison is in the opposite direction from to the global tropical (<15°N/S) P-E change in the same model (Cramwinckel et al., 2023), which shows an overall P-E decrease (drier conditions). This suggests that the response observed at Site 1258 is likely due to regional, not global effects.

Regionally, an obvious exception to the global pattern of enhanced low-latitude evaporation with warming is found in the ITCZ. The ITCZ is an area within 5 degrees of latitude of the equator (on an annual basis) where the convergence of the trade winds drives intense precipitation and, therefore, a regionally lower sea-surface $\delta^{18}O$ (e.g., LeGrande & Schmidt, 2006). The ITCZ migrates north and south with the seasons, and Site 1258 is located near the maximum Northern Hemisphere summer seasonal latitudinal extreme of the ITCZ (both in the modern, Schlosser et al., 2014, and on Eocene paleogeography as modeled in iCESM1.2, Zhu et al., 2020) and on an annual basis currently experiences net evaporation (e.g., Yoo & Carton, 1990). Recent literature has suggested that anthropogenic climate change is altering the path of the ITCZ, causing it to vary regionally in width and latitudinal position, with specific regional responses controlled by continental configuration (Bischoff & Schneider, 2014; Bryne et al., 2018; Donohoe et al., 2013; Mamalakis et al., 2021). During the extreme warmth of the PETM, northward migration or narrowing of the ITCZ into the Site 1258 region could have driven more local precipitation, lowering the $\delta^{18}O$ of seawater. Previous work has offered different conclusions about changes to the ITCZ in response to Eocene warming: Tierney et al. (2022) suggested a narrowing of the ITCZ during the PETM, while Cramwinckel et al. (2023), focusing more broadly on the Early Eocene Climatic Optimum, argues that modeled narrowing of the ITCZ is not supported by tropical paleoproxy data. GCM modeling by Acosta et al. (2022) argue that increasing pCO_2 in the Early Eocene led to a strengthened ITCZ, but did not significantly alter the position of monsoonal precipitation.

Enhanced continental runoff is another potential mechanism for the lower $\delta^{18}O$ value seen in both our PETM record and isotope-enabled climate modeling. Today, Site 1258 is located only 400 km north of the South American continent (and would have been a similar distance during the PETM), close enough that the plume of freshwater from Amazon river discharge periodically extends to the surface waters overlying Site 1258 (Grodsky et al., 2014; Shi & Wang, 2024). South American continental runoff has a distinctly lower (by several permil) $\delta^{18}O$ value than open-ocean tropical Atlantic surface seawater (Karr & Showers, 2002). While the modern Amazon river has only existed as a transcontinental system with headwaters in the Eastern Andes since the mid-Miocene (Figueiredo et al., 2009), Eocene paleogeographic reconstructions (including that used by iCESM, Herold et al., 2014) show large areas of northern South America draining to the northeast, toward the Site 1258 region. If precipitation over northern South America was significantly enhanced during the warmth of the PETM, this could have increased continental runoff to such an extent that SSS and $\delta^{18}O$ values were reduced at Site 1258. Palynological records from Columbia and Venezuela suggest a significant increase in plant diversity during the PETM, and an increase in morphotypes common in wet tropical rainforest, suggesting greater precipitation during the event (Jaramillo et al., 2010). Paleosols from the same Columbian section show evidence for increased chemical weathering and a lack of carbonate nodules, both of which were interpreted as evidence for increased precipitation (Morón et al., 2013), presumably due to enhanced ITCZ precipitation and/or enhanced South American monsoonal precipitation (Huber & Goldner, 2012). Either ITCZ narrowing/migration or enhanced continental runoff, or a combination of the two, could be the cause of the lower $\delta^{18}O$ value of tropical Atlantic seawater seen in the latter stages of the PETM in our new reconstruction from Site 1258.

5. Conclusions

The results of this study represent the first sea surface paleotemperature and seawater oxygen isotope reconstructions across the PETM from deep-sea sediments in the tropical Atlantic. Our coupled Mg/Ca and $\delta^{18}O$-based paleotemperature record demonstrates a pronounced, rapid warming of $4.9 \pm \frac{0.4}{0.5}$ °C coincident with the PETM CIE. Warm conditions endured for close to 100 kyr before gradually recovering to near pre-event temperatures over the subsequent ~100 kyr. The magnitude and timing of rapid warming, a period of sustained warmth, and then gradual recovery are all consistent with other PETM paleotemperature records from the tropics (Frieling et al., 2017; Tripati & Elderfield, 2005; Zachos et al., 2003) and elsewhere (Dunkley-Jones et al., 2013). Comparing the magnitude of warming in our paleotemperature reconstructions with modeled regional temperature fields under elevated pCO_2 bolsters support for model skill in reproducing sea surface temperatures under greenhouse climates.

However, the response of tropical Atlantic hydroclimate, as constrained by reconstructed seawater oxygen isotopic composition and salinity, are not as straight forward. Our reconstruction of surface seawater $\delta^{18}O$ shows little change at the onset of the PETM, followed by a decrease in seawater $\delta^{18}O$ during the later stages of the event —the opposite of what would generally be expected for the tropics under the typical "wet-get-wetter, dry-get-drier" conceptual model. Intriguingly, some support for a complex, non-linear response of seawater $\delta^{18}O$ to extreme greenhouse climates is found in recent isotope-enabled climate modeling (Zhu et al., 2020). Under extremely elevated pCO_2, modeled seawater $\delta^{18}O$ in the Site 1258 region also declines, hinting at a non-linear regional response in extreme greenhouse climates. Taken together, both the model and the data seem to suggest that a threshold may exist at very high pCO_2/temperature, above which the hydrologic response in the Site 1258 region becomes insensitive to further warming, and even reverses. The reasons for this complex response are uncertain at present, but we speculate that it could be related to the narrowing or migration of the ITCZ, or enhanced continental runoff from South America under extreme greenhouse conditions. Such unexpected regional complexities in the response of the hydrologic cycle to greenhouse warming present a challenge for predictions of precipitation and evaporation redistribution under future climate change.

Data Availability Statement

All geochemical data (foraminiferal $\delta^{18}O$ and Mg/Ca) are included in Table S1 in Supporting Information S1, and archived in the Pangaea online data respository (Penman & Howard, 2025). The Bayesian proxy system model used here is publicly available through Zenodo (Harper, 2024).

Acknowledgments
This study was funded by National Science Foundation (NSF) Award OCE-2202983 to D. Penman. Samples used in this study were collected as part of Ocean Drilling Program (ODP) Leg 207. The Community Earth System Model project is supported primarily by the NSF. This material is based upon work supported by NSF and the National Center for Atmospheric Research, which is a major facility sponsored by the NSF under Cooperative Agreement No. 1852977. We thank reviewers Tom Dunkley Jones and Tobias Agterhuis as well as Editor Matthew Huber and Associate Editor Alex Farnsworth for their thoughtful suggestions which improved the manuscript.

References

Abbot, D. S., Huber, M., Bousquet, G., & Walker, C. C. (2009). High-CO2 cloud radiative forcing feedback over both land and ocean in a global climate model. *Geophysical Research Letters*, *36*, 5. https://doi.org/10.1029/2008gl036703

Acosta, R. P., Ladant, J. B., Zhu, J., & Poulsen, C. J. (2022). Evolution of the Atlantic Intertropical Convergence Zone, and the South American and African monsoons over the past 95-Myr and their impact on the tropical rainforests. *Paleoceanography and Paleoclimatology*, *37*(7), e2021PA004383. https://doi.org/10.1029/2021pa004383

Aze, T., Pearson, P. N., Dickson, A. J., Badger, M. P., Bown, P. R., Pancost, R. D., et al. (2014). Extreme warming of tropical waters during the Paleocene–Eocene Thermal Maximum. *Geology*, *42*(9), 739–742. https://doi.org/10.1130/g35637.1

Barker, S., Greaves, M., & Elderfield, H. (2003). A study of cleaning procedures used for foraminiferal Mg/Ca paleothermometry. *Geochemistry, Geophysics, Geosystems*, *4*(9), 8407. https://doi.org/10.1029/2003GC000559

Birch, H. S., Coxall, H. K., & Pearson, P. N. (2012). Evolutionary ecology of Early Paleocene planktic foraminifera: Size, depth habitat, and symbiosis. *Paleobiology*, *38*(3), 374–390. https://doi.org/10.1666/11027.1

Bischoff, T., & Schneider, T. (2014). Energetic constraints on the position of the intertropical convergence zone. *Journal of Climate*, *27*(13), 4937–4951. https://doi.org/10.1175/jcli-d-13-00650.1

Bowen, G. J., Fischer-Femal, B., Reichart, G. J., Sluijs, A., & Lear, C. H. (2020). Joint inversion of proxy system models to reconstruct paleoenvironmental time series from heterogeneous data. *Climate of the Past*, *16*(1), 65–78. https://doi.org/10.5194/cp-16-65-2020

Bryne, M. P., Pendergrass, A. G., Rapp, A. D., & Wodzicki, K. R. (2018). Response of the Intertropical Convergence Zone to Climate Change: Location, width, and strength. *Current Climate Change Reports*, *4*, 355–370. https://doi.org/10.1007/s40641-018-0110-5

Burke, E. J., Brown, S. J., & Christidis, N. (2006). Modeling the recent evolution of global drought and projects for the twenty-first century with the Hadley Centre Climate Model. *Journal of Hydrometeorology*, *7*(5), 1113–1125. https://doi.org/10.1175/jhm544.1

Caballero, R., & Huber, M. (2010). Spontaneous transition to superrotation in warm climates simulated by CAM3. *Geophysical Research Letters*, *37*, 11. https://doi.org/10.1029/2010gl043468

Carmichael, M. J., Inglis, G. N., Badger, M. P. S., Naafs, B. D. A., Behrooz, L., Remmelzwaal, S., et al. (2017). Hydrological and associated biogeochemical consequences of rapid global warming during the Paleocene-Eocene Thermal Maximum. *Global and Planetary Change*, *157*, 114–138. https://doi.org/10.1016/j.gloplacha.2017.07.014

Cramer, B. S., Miller, K. G., Barrett, P. J., & Wright, J. D. (2011). Late Cretasceous-Neogene trends in deep ocean temperature and continental ice volume: Recoiling records of benthic foraminiferal geochemistry (δ^{18}O and Mg/Ca) wit sea level history. *Journal of Geophysical Research*, *116*, 1–23.

Cramwinckel, M. J., Burls, N. J., Fahad, A. A., Knapp, S., West, C. K., Reichgelt, T., et al. (2023). Global and zonal-mean hydrological response to early Eocene warmth. *Paleoceanography and Paleoclimatology*, *38*(6), e2022PA004542. https://doi.org/10.1029/2022pa004542

Daëron, M., Drysdale, R. N., Peral, M., Huyghe, D., Blamart, D., Coplen, T. B., et al. (2019). Most Earth-surface calcites precipitate out of isotopic equilibrium. *Nature Communications*, *10*(1), 429. https://doi.org/10.1038/s41467-019-08336-5

Dee, S., Bailey, A., Conroy, J., Atwood, A., Stevenson, S., Nusbaumer, J., & Noon, D. (2023). Water isotopes, climate variability, and the hydrologic cycle: Recent advances and new frontiers. *Environmental Research Climate*, *2*, 1–29.

Dee, S., Emile-Geay, J., Evans, M. N., Allam, A., Steig, E. J., & Thompson, D. M. (2015). PRYSM: An open-source framework for PRoxY System Modeling, with applications to oxygen-isotope systems. *Journal of Advances in Modeling Earth Systems*, *7*(3), 1220–1247. https://doi.org/10.1002/2015ms000447

Delaney, M. L., Be, A. W. H., & Boyle, E. A. (1985). Li, Sr, Mg, and Na in foraminiferal calcite shells from laboratory culture, sediment traps, and sediment cores. *Geochimica et Cosmochimica Acta*, *49*(6), 1327–1341. https://doi.org/10.1016/0016-7037(85)90284-4

Dickens, G. R., Castillo, M. M., & Walker, J. C. G. (1997). A blast of gas in the latest Paleocene: Simulating first-order effects of massive dissociation of oceanic methane hydrate. *Geology*, *25*(30), 259–262. https://doi.org/10.1130/0091-7613(1997)025<0259:abogit>2.3.co;2

Dickens, G. R., O'Niel, J. R., Rea, D. K., & Owen, R. M. (1995). Dissociation of oceanic methane hydrate as a cause for the carbon isotope excursion at the end of the Paleocene. *Paleoceanography*, *10*(6), 965–971.

Donohoe, A., Marshall, J., Ferreira, D., & McGee, D. (2013). The relationship between ITCZ location and cross-equatorial atmospheric heat transport: From the seasonal cycle to the last glacial maximum. *Journal of Climate*, *26*(11), 3597–3618. https://doi.org/10.1175/jcli-d-12-00467.1

Dunkley-Jones, T., Lunt, D. J., Schmidt, D. N., Ridgwell, A., Sluijs, A., Valdes, P. J., & Maslin, M. (2013). Climate model and proxy data constraints on ocean warming across the Paleocene–Eocene Thermal Maximum. *Earth-Science Reviews*, *125*, 123–145. https://doi.org/10.1016/j.earscirev.2013.07.004

Erbacher, J., Mosher, D. C., Malone, M. J., Sexton, P., & Wilson, P. A. (2004). *Proceedings of the Ocean Drilling Program, Initial Reports. Vol. 207. Demerera Rise: equatorial Cretaceous and Paleogene paleoceanographic transect, Western Australia. Covering Leg 207 of the cruises of the Drilling Vessel "Joides Resolution", Bridgetown, Barbados, to Rio de Janeiro, Brazil, Sites 1257-1261, 11 January-6 March 2003* (Proceedings of the Ocean Drilling Program, Initial Reports, 207), (Vol. 207, p. 89). Texas A & M University Ocean Drilling Program.

Evans, D., Wade, B. S., Henehan, M., Erez, J., & Miller, W. (2016). Revisiting carbonate chemistry controls on planktic foraminifera Mg/Ca: Implications for sea surface temperature and hydrology shifts over the Paleocene-Eocene Thermal Maximum and Eocene-Oligocene transition, 2015. *Climate of the Past*, *12*(4), 819–835. https://doi.org/10.5194/cp-12-819-2016

Evans, M. N., Tolwinski-Ward, S. E., Thompson, D. M., & Anchukaitis, K. J. (2013). Applications of proxy system modeling in high resolution paleoclimatology. *Quaternary Science Reviews*, *76*, 16–28. https://doi.org/10.1016/j.quascirev.2013.05.024

Farley, K. A., & Eltgroth, S. F. (2003). An alternative age model for the Paleocene–Eocene thermal maximum using extraterrestrial 3He. *Earth and Planetary Science Letters*, *208*(3–4), 135–148. https://doi.org/10.1016/s0012-821x(03)00017-7

Figueiredo, J. J. J. P., Hoorn, C., Van der Ven, P., & Soares, E. (2009). Late Miocene onset of the Amazon River and the Amazon deep-sea fan: Evidence from the Foz do Amazonas Basin. *Geology*, *37*(7), 619–622. https://doi.org/10.1130/g25567a.1

Frieling, J., Gebhardt, H., Huber, M., Adekeye, O. A., Akande, S. O., Reichart, G. J., et al. (2017). Extreme warmth and heat-stressed plankton in the tropics during the Paleocene-Eocene Thermal Maximum. *Science Advances*, *3*(3), e1600891. https://doi.org/10.1126/sciadv.1600891

Frieling, J., Reichart, G. J., Middelburg, J. J., Röhl, U., Westerhold, T., Bohaty, S. M., & Sluijs, A. (2018). Tropical Atlantic climate and ecosystem regime shifts during the Paleocene–Eocene Thermal Maximum. *Climate of the Past*, *14*(1), 39–55. https://doi.org/10.5194/cp-14-39-2018

Gaskell, D. E., Huber, M., O'Brien, C. L., Inglis, G. N., Acosta, R. P., Poulsen, C. J., & Hull, P. M. (2022). The latitudinal temperature gradient and its climate dependence as inferred from foraminiferal δ18O over the past 95 million years. *Proceedings of the National Academy of Sciences*, *119*(11), e2111332119. https://doi.org/10.1073/pnas.2111332119

Gray, W. R., & Evans, D. (2019). Nonthermal influences on Mg/Ca in planktonic foraminifera: A review of culture studies and application to the last glacial maximum. *Paleoceanography and Paleoclimatology*, *34*(3), 306–315. https://doi.org/10.1029/2018pa003517

Gregory, J. M., Mitchell, J. F. B., & Brady, A. J. (1997). Summer drought in northern midlatitudes in a time-dependent CO_2 climate experiment. *Journal of Climate*, *10*(4), 662–686. https://doi.org/10.1175/1520-0442(1997)010<0662:sdinmi>2.0.co;2

Grodsky, S. A., Reverdin, G., Carton, J. A., & Coles, V. J. (2014). Year-to-year salinity changes in the Amazon plume: Contrasting 2011 and 2012 Aquarius/SACD and SMOS satellite data. *Remote Sensing of Environment*, *140*, 14–22. https://doi.org/10.1016/j.rse.2013.08.033

Gutjahr, M., Ridgwell, A., Sexton, P. F., Anagnostou, E., Pearson, P. N., Palike, H., et al. (2017). Very large release of mostly volcanic carbon during the Palaeocene-Eocene Thermal Maximum. *Nature*, *548*(7669), 573–577. https://doi.org/10.1038/nature23646

Harper, D. T. (2024). Bayesian proxy system model for reconstructing PETM sea surface temperature and salinity at ODP Site 1258 [Software]. *Zenodo*. https://doi.org/10.5281/zenodo.11225129

Harper, D. T., Hönisch, B., Bowen, G. J., Zeebe, R. E., Haynes, L. L., Penman, D. E., & Zachos, J. C. (2024). Long-and short-term coupling of sea surface temperature and atmospheric CO2 during the late Paleocene and early Eocene. *Proceedings of the National Academy of Sciences*, *121*(36), e2318779121. https://doi.org/10.1073/pnas.2318779121

Haynes, L. L., Hönisch, B., Holland, K., Eggins, S., & Rosenthal, Y. (2023). Calibrating non-thermal effects on planktic foraminiferal Mg/Ca for application across the Cenozoic. *Paleoceanography and Paleoclimatology*, *38*(10), e2023PA004613. https://doi.org/10.1029/2023pa004613

Held, I. S., & Soden, B. J. (2000). Water vapor feedback and global warming. *Annual Review of Energy and the Environment*, *25*(1), 441–475. https://doi.org/10.1146/annurev.energy.25.1.441

Held, I. S., & Soden, B. J. (2005). Robust response of the hydrologic cycle to global warming. *Journal of Climate*, *19*(21), 5686–5699. https://doi.org/10.1175/jcli3990.1

Herold, N., Buzan, J., Seton, M., Goldner, A., Green, J. A. M., Müller, R. D., et al. (2014). A suite of early Eocene (~55 Ma) climate model boundary conditions. *Geoscientific Model Development*, *7*(5), 2077–2090. https://doi.org/10.5194/gmd-7-2077-2014

Hollis, C. J., Jones, T. D., Anagnostou, E., Bijl, P. K., Cramwinckel, M. J., Cui, Y., et al. (2019). The DeepMIP contribution to PMIP4: Methodologies for selection, compilation and analysis of latest Paleocene and early Eocene climate proxy data, incorporating version 0.1 of the DeepMIP database. *Geoscientific Model Development*, *12*(7), 3149–3206. https://doi.org/10.5194/gmd-12-3149-2019

Hönisch, B., Andy Ridgwell, A., Daniela, N., Schmidt, N. D., Ellen Thomas, E., Gibbs, S. J., et al. (2012). The geologic record of ocean acidification. *Science*, *335*(6072), 1058–1063. https://doi.org/10.1126/science.1208277

Horita, J., Rozanski, K., & Cohen, S. (2008). Isotope effects in the evaporation of water: A status report of the Craig–Gordon model. *Isotopes in Environmental and Health Studies*, *44*(1), 23–49. https://doi.org/10.1080/10256010801887174

Huber, M., & Goldner, A. (2012). Eocene monsoons. *Journal of Asian Earth Sciences*, *44*, 3–23. https://doi.org/10.1016/j.jseaes.2011.09.014

Inglis, G. N., Bragg, F., Burls, N., Evans, D., Foster, G. L., Huber, M., et al. (2020). Global mean surface temperature and climate sensitivity of the EECO, PETM and latest Paleocene. *Climate of the Past Discussions*, *2020*, 1–43.

IPCC. (2023). Climate change 2023: Synthesis report. In H. Lee & J. Romero (Eds.), *Contribution of Working Groups I, II and III to the Sixth Assessment Report of the Intergovernmental Panel on Climate Change [Core Writing Team* (pp. 35–115). IPCC.

Jaramillo, C., Ochoa, D., Contreras, L., Pagani, M., Carvajal-Ortiz, H., Pratt, L. M., et al. (2010). Effects of rapid global warming at the Paleocene-Eocene boundary on neotropical vegetation. *Science*, *330*(6006), 957–961. https://doi.org/10.1126/science.1193833

Karr, J. D., & Showers, W. J. (2002). Stable oxygen and hydrogen isotopic tracers in Amazon shelf waters during Amasseds. *Oceanologica Acta*, *25*(2), 71–78. https://doi.org/10.1016/s0399-1784(02)01183-0

Katz, M. E., Pak, D. K., Dickens, G. R., & Miller, K. G. (1999). The source and fate of massive carbon input during the latest Paleocene thermal maximum. *Science*, *286*(5444), 1531–1533. https://doi.org/10.1126/science.286.5444.1531

Kelly, D. C., Bralower, T. J., & Zachos, J. C. (2001). On the demise of the early Paleogene Morozovella velascoensis lineage: Terminal progenesis in the planktic foraminifera. *Society for Sedimentary Geology*, *16*(5), 507–523. https://doi.org/10.2307/3515565

Kennett, J. P., & Stott, L. D. (1991). Abrupt deep-sea warming, palaeoceanographic changes and benthic extinctions at the end of the Paleocene. *Nature*, *353*(6341), 225–229. https://doi.org/10.1038/353225a0

Kim, S. T., Copland, T. B., & Horita, J. (2015). Normalization of stable isotope data for carbonate minerals: Implications of IUPAC guidelines. *Geochimica et Cosmochimica Acta*, *158*, 276–289.

Kirtland Turner, S. (2018). Constraints on the onset duration of the Paleocene–Eocene Thermal Maximum. *Philosophical Transactions of the Royal Society A: Mathematical, Physical & Engineering Sciences*, *376*(2130), 20170082. https://doi.org/10.1098/rsta.2017.0082

Kirtland Turner, S., & Ridgwell, A. (2016). Development of a novel empirical framework for interpreting geological carbon isotope excursions, with implications for the rate of carbon injection across the PETM. *Earth and Planetary Science Letters*, *435*, 1–13. https://doi.org/10.1016/j.epsl.2015.11.027

Koch, P. L., Zachos, J. C., & Gingerich, P. D. (1992). Correlation between isotope records in marine and continental carbon reservoirs neat the Palaeocene/Eocene boundary. *Nature*, *358*(6384), 319–322. https://doi.org/10.1038/358319a0

Kozdon, R., Kelly, D. C., Kitajima, K., Strickland, A., Fournelle, J. H., & Valley, J. W. (2013). In situ $\delta^{18}O$ and Mg/Ca analyses of diagenetic and planktic foraminiferal calcite preserved in a deep-sea record of the Paleocene-Eocene thermal maximum. *Paleoceanography*, *28*(3), 517–528. https://doi.org/10.1002/palo.20048

Kurtz, A. C., Kump, L. R., Arthur, M. A., Zachos, J. C., & Paytan, A. (2003). Early Cenozoic decoupling of the global carbon and sulfur cycles. *Paleoceanography*, *18*(4). 14,1-14,14. https://doi.org/10.1029/2003pa000908

Kvenolden, K. A. (1993). Gas hydrates – Geological perspective and global change. *American Geophysical Union: Reviews of Geophysics*, *31*(2), 173–187. https://doi.org/10.1029/93rg00268

Lear, C. H., Elderfield, H., & Wilson, P. A. (2000). Cenozoic deep-sea temperatures and global ice volumes from Mg/Ca in benthic foraminiferal calcite. *Science*, *287*(5451), 269–272. https://doi.org/10.1126/science.287.5451.269

LeGrande, A. N., & Schmidt, G. A. (2006). Global gridded data set of the oxygen isotopic composition in seawater. *Geophysical Research Letters*, *33*(12). https://doi.org/10.1029/2006gl026011

Liu, C., Liao, X., Qiu, J., Yang, Y., Feng, X., Allan, R. P., et al. (2020). Observed variability of intertropical convergence zone over 1998-2018. *Environmental Research Letters*, *15*(10), 1–13. https://doi.org/10.1088/1748-9326/aba033

Mamalakis, A., Randerson, J. T., Jin-Yi, Y., Pritchard, M. S., Magnusdottir, G., Smyth, P., et al. (2021). Zonally contrasting shifts of the tropical rain belt in response to climate change. *Nature Climate Change*, *11*(2), 143–151. https://doi.org/10.1038/s41558-020-00963-x

Manabe, S., Wetherald, R. T., Milly, P. C. D., Delworth, T. L., & Stouffer, R. J. (2004). Century-scale change in water availability: CO_2-quadrupling experiment. *Climatic Change*, *64*(1/2), 59–76. https://doi.org/10.1023/b:clim.0000024674.37725.ca

Mashiotta, T. A., Lea, D. W., & Howard, S. J. (1999). Glacial-interglacial changes in subantarctic sea surface temperature and $\delta^{18}O$-water using foraminiferal Mg. *Earth and Planetary Science Letters*, *170*(4), 417–432. https://doi.org/10.1016/s0012-821x(99)00116-8

McInerney, F. A., & Wing, S. L. (2011). The Paleocene-Eocene Thermal Maximum: A perturbation of carbon cycle, climate, and biosphere with implications for the future. *Annual Review of Earth and Planetary Sciences*, *39*(1), 489–516. https://doi.org/10.1146/annurev-earth-040610-133431

Morón, S., Fox, D. L., Feinberg, J. M., Jaramillo, C., Bayona, G., Montes, C., & Bloch, J. I. (2013). Climate change during the Early Paleogene in the Bogotá Basin (Colombia) inferred from paleosol carbon isotope stratigraphy, major oxides, and environmental magnetism. *Palaeogeography, Palaeoclimatology, Palaeoecology*, *388*, 115–127. https://doi.org/10.1016/j.palaeo.2013.08.010

Myhre, G., Alterskjær, K., Stjern, C. W., Hodnebrog, Ø., Marelle, L., Samset, B. H., et al. (2019). Frequency of extreme precipitation increases extensively with event rareness under global warming. *Scientific Reports*, *9*(1), 16063. https://doi.org/10.1038/s41598-019-52277-4

Nunes, F., & Norris, R. D. (2006). Abrupt reversal in ocean overturning during the Palaeocene/Eocene warm period. *Nature*, *439*(7072), 60–63. https://doi.org/10.1038/nature04386

O'Gorman, P. A., & Schneider, T. (2008). The hydrological cycle over a wide range of climates simulated with an idealized GCM. *Journal of Climate*, *21*(15), 3815–3832. https://doi.org/10.1175/2007jcli2065.1

Pagani, M., Calderia, K., Archer, D., & Zachos, J. C. (2006). An ancient carbon mystery. *Science*, *314*(5805), 1556–1557. https://doi.org/10.1126/science.1136110

Pälike, C., Delaney, M. L., & Zachos, J. C. (2014). Deep-sea redox across the Paleocene-Eocene thermal maximum. *Geochemistry, Geophysics, Geosystems*, *15*(4), 1038–1053. https://doi.org/10.1002/2013gc005074

Paul, D., & Skrzyoek, G. (2007). Assessment of carbonate-phosphoric acid analytical technique performed using GasBench II in continuous flow isotope ratio mass spectrometry. *International Journal of Mass Spectrometry*, *262*(3), 180–186. https://doi.org/10.1016/j.ijms.2006.11.006

Pearson, P. N. (2012). *Oxygen isotopes in foraminifera: Overview and historical review* (Vol. 18, 1–38). The Paleontological Society Press. https://doi.org/10.1017/s1089332600002539

Penman, D. E., Honish, B., Zeebe, R. E., Thomas, E., & Zachos, J. C. (2014). Rapid and sustained surface ocean acidification during the Paleocene-Eocene Thermal Maximum. *Paleoceanography and Paleoclimatology*, *29*(5), 357–369. https://doi.org/10.1002/2014PA002621

Penman, D. E., & Howard, C. (2025). Foraminiferal geochemical data across the Paleocene-Eocene Thermal Maximum from IODP Site 1258 [dataset]. *PANGAEA*. https://doi.org/10.1594/PANGAEA.977805

Plummer, M. (2003). JAGS: A program for analysis of Bayesian graphical models using Gibbs sampling. *Proceedings of the 3rd international workshop on distributed statistical computing*, *124*(125.10), 1–10.

R Core Team, R. (2013). R: A language and environment for statistical computing.

Röhl, U., Westerhold, T., Bralower, T. J., & Zachos, J. C. (2007). On the duration of the Paleocene-Eocene thermal maximum (PETM). *Geochemistry, Geophysics, Geosystems*, *8*, 12. https://doi.org/10.1029/2007gc001784

Schlosser, C., Klar, J. K., Wake, B. D., Snow, J. T., Honey, D. J., Woodward, E. M. S., et al. (2014). Seasonal ITCZ migration dynamically controls the location of the (sub) tropical Atlantic biogeochemical divide. *Proceedings of the National Academy of Sciences*, *111*(4), 1438–1442. https://doi.org/10.1073/pnas.1318670111

Sexton, P. F., Wilson, P. A., & Pearson, P. N. (2006). Microstructural and geochemical perspectives on planktic foraminiferal preservation: "Glassy" versus "Frosty". *Geochemistry, Geophysics, Geosystems*, *7*(12). https://doi.org/10.1029/2006gc001291

Shi, W., & Wang, M. (2024). Monitoring the Amazon River plume from satellite observations. *GIScience and Remote Sensing*, *61*(1), 2416725. https://doi.org/10.1080/15481603.2024.2416725

Sluijs, A., Rohl, U., Schouten, S., Brumsack, H. J., Sangiori, F., Sinninghe Damste, J. S., & Brinkhuis, H. (2008). Artic late Paleocene-early Eocene paleoenvironments with special emphasis on the Paleocene-Eocene thermal maximum (Lomonosov Ridge, Integrated Ocean Drilling Program Expedition 302). *Paleoceanography*, *23*, 1–17. https://doi.org/10.1029/2007pa001495

Sluijs, A., Schouten, S., Pagani, M., Woltering, M., Brinkhuis, H., Sinninghe Damste, J. S., et al. (2006). Subtropical Artic Ocean temperatures during the Palaeocene/Eocene thermal maximum. *Nature*, *441*(7093), 610–613. https://doi.org/10.1038/nature04668

Su, Y. S., & Yajima, M. (2015). R2jags: Using R to run 'JAGS'. R package version 0.5-7, 34.

Svensen, H., Planke, S., & Corfu, F. (2010). Zircon dating ties NE Atlantic sill emplacement to initial Eocene global warming. *Journal of the Geological Society, London*, *167*(3), 433–436. https://doi.org/10.1144/0016-76492009-125

Svensen, H., Planke, S., Malthe-Sorenssen, A., Jamtveit, B., Myklebust, R., Eldem, T. R., & Rey, S. S. (2004). Release of methane from a volcanic basin as a mechanism for initial Eocene global warming. *Nature*, *429*(6991), 542–545. https://doi.org/10.1038/nature02566

Tierney, J. E., Zhu, J., Li, M., Ridgwell, A., Hakim, G. J., Poulsen, C. J., et al. (2022). Spatial patterns of climate change across the Paleocene–Eocene Thermal Maximum. *Proceedings of the National Academy of Sciences*, *119*(42), e2205326119. https://doi.org/10.1073/pnas.2205326119

Tingley, M. P., Craigmile, P. F., Haran, M., Li, B., Mannshardt, E., & Rajaratnam, B. (2012). Piecing together the past: Statistical insights into paleoclimatic reconstructions. *Quaternary Science Reviews*, *35*, 1–22. https://doi.org/10.1016/j.quascirev.2012.01.012

Tripati, A., & Elderfield, H. (2005). Deep-sea temperature and circulation changes at the Paleocene-Eocene thermal maximum. *Science*, *308*(5730), 1894–1898. https://doi.org/10.1126/science.1109202

Wade, B. S., Houben, A. J. P., Willemijn, Q., Schouten, S., Rosenthal, Y., Miller, K. G., et al. (2012). Multiproxy record of abrupt sea-surface cooling across the Oligocene transition in the Gulf of Mexico. *Geology*, *40*(2), 159–162.

Walters, G. L., Kemp, S. J., Hemingway, J. D., Johnston, D. T., & Hodell, D. A. (2022). Clay hydroxyl isotopes show an enhanced hydrologic cycle during the Paleocene-Eocene Thermal Maximum. *Nature Communications*, *13*(1), 7885. https://doi.org/10.1038/s41467-022-35545-2

Wang, G. (2005). Agricultural drought in a future climate: Results from 15 global climate models participating in the IPCC 4th assessment. *Climate Dynamics*, *25*(7–8), 739–753. https://doi.org/10.1007/s00382-005-0057-9

Westerhold, T., Rohl, U., McCarren, H. K., & Zachos, J. C. (2009). Latest on the absolute age of the Paleocene-Eocene Thermal Maximum (PETM): New insights from exact stratigraphic position of key ash layers +19 and -17. *Earth and Planetary Science Letters*, *2887*(3–4), 412–419. https://doi.org/10.1016/j.epsl.2009.08.027

Yoo, J. M., & Carton, J. A. (1990). Annual and interannual variation of the freshwater budget in the tropical Atlantic Ocean and the Caribbean Sea. *Journal of Physical Oceanography*, *20*(6), 831–845. https://doi.org/10.1175/1520-0485(1990)020<0831:aaivot>2.0.co;2

Zachos, J. C., Rohl, U., Schellenber, S. A., Sluijs, A., Hodell, D. A., Kelly, D. C., et al. (2005). Rapid acidification of the ocean during the Paleocene-Eocene thermal maximum. *Science*, *308*(5728), 1611–1615. https://doi.org/10.1126/science.1109004

Zachos, J. C., Wara, M. W., Boharty, S., Delaney, M. L., Petrizzo, M. R., Brill, A., et al. (2003). A transient rise in tropical sea surface temperature during the Paleocene-Eocene Thermal Maximum. *Science*, *302*(5650), 1551–1554. https://doi.org/10.1126/science.1090110

Zeebe, R. E., Ridgwell, A., & Zachos, J. C. (2016). Anthropogenic carbon release rate unprecedented during the past 66 million years. *Nature Geoscience*, *9*(4), 325–329. https://doi.org/10.1038/ngeo2681

Zeebe, R. E., & Zachos, J. C. (2007). Reversed deep-sea carbonate ion basin gradient during Paleocene-Eocene thermal maximum. *Paleoceanography*, *22*(3). https://doi.org/10.1029/2006pa001395

Zeebe, R. E., Zachos, J. C., & Dickens, G. R. (2009). Carbon dioxide forcing alone insufficient to explain Palaeocene-Eocene Thermal Maximum. *Nature Geoscience*, *2*(8), 576–580. https://doi.org/10.1038/ngeo578

Zhu, J., Poulsen, C. J., Otto-Bliesner, B. L., Liu, Z., Brady, E. C., & Noone, D. C. (2020). Simulation of early Eocene water isotopes using an Earth system model and its implication for past climate reconstruction. *Earth and Planetary Science Letters*, *537*, 1–11. https://doi.org/10.1016/j.epsl.2020.116164